PHYSICAL REVIEW D **89,** 103515 (2014)

Large-scale structure formation with massive neutrinos and dynamical dark energy

Amol Upadhye,[1,2] Rahul Biswas,[1] Adrian Pope,[1] Katrin Heitmann,[1,2,3] Salman Habib,[1,2,3] Hal Finkel,[4] and Nicholas Frontiere[1,5]

[1]*High Energy Physics Division, Argonne National Laboratory, 9700 S. Cass Avenue, Lemont, Illinois 60439, USA*
[2]*Kavli Institute for Cosmological Physics, The University of Chicago, Chicago, Illinois 60637, USA*
[3]*Mathematics and Computer Science Division, Argonne National Laboratory, 9700 South Cass Avenue, Lemont, Illinois 60439, USA*
[4]*ALCF, Argonne National Laboratory, 9700 S. Cass Avenue, Lemont, Illinois 60439, USA*
[5]*Department of Physics, The University of Chicago, Chicago, Illinois 60637, USA*
(Received 26 September 2013; published 13 May 2014)

Over the next decade, cosmological measurements of the large-scale structure of the Universe will be sensitive to the combined effects of dynamical dark energy and massive neutrinos. The matter power spectrum is a key repository of this information. We extend higher-order perturbative methods for computing the power spectrum to investigate these effects over quasilinear scales. Through comparison with N-body simulations, we establish the regime of validity of a time-renormalization group perturbative treatment that includes dynamical dark energy and massive neutrinos. We also quantify the accuracy of standard, renormalized and Lagrangian resummation (LPT) perturbation theories without massive neutrinos. We find that an approximation that neglects neutrino clustering as a source for nonlinear matter clustering predicts the baryon acoustic oscillation (BAO) peak position to 0.25% accuracy for redshifts $1 \leq z \leq 3$, justifying the use of LPT for BAO reconstruction in upcoming surveys. We release a modified version of the public CORTER code which includes the additional physics discussed in the paper.

DOI: 10.1103/PhysRevD.89.103515 PACS numbers: 98.80.-k, 98.65.Dx, 14.60.Pq, 95.36.+x

I. INTRODUCTION

A. Dynamical dark energy and neutrinos

The original discovery of the late-time acceleration of the Universe [1,2] has been confirmed by multiple cosmological probes over the last fifteen years. The underlying cause of this acceleration, as well as its connection to fundamental physics, however, remains to be clarified. Although the cosmological standard model provides an excellent description of the latest data [3–11], the cosmological constant is beset with problems of extreme fine-tuning, at least given our current level of theoretical understanding (for reviews see, Refs. [12–16]). For this reason, it is extremely important to constrain the evolution of the dark energy equation of state, and to see if the associated equation of state parameter, $w(z)$, deviates from the constant value, $w = -1$, characteristic of a cosmological constant. While phenomenological models for $w(z)$ can be postulated for comparison to observed data, one class of solutions known as early dark energy allows for the energy density responsible for the acceleration to be much larger at earlier times, with possible connections to fundamental physics [17–24].

Investigations of dynamical dark energy are conducted using two distinct types of observational probes: (i) constraints on the homogeneous expansion of the Universe, and (ii) the growth of large-scale structure, driven primarily by the gravitational dynamics of cold dark matter (CDM). Via consistency relations, these results can also be used to study the validity of general relativity in describing the dynamics of the Universe (see, e.g., Ref. [25]), although this is not our concern here.

Besides dark energy, a major contribution of modern cosmology to fundamental physics lies in constraining the sum of neutrino masses, as well as the number of neutrino species. Massive neutrinos act as a radiation component in the early universe, but as a warm dark matter fluid at late times. The high velocity of neutrinos makes them difficult to bind gravitationally, suppressing the growth of structure in a scale-dependent manner. Aside from being interesting in their own right, massive neutrinos can be degenerate with the dark energy density and the equation of state [26], which necessitates an analysis including both effects. Therefore, it is essential for future precision measurements to include neutrinos as a component of the analysis, along with a time-varying dark energy equation of state or a modified theory of gravity. A thorough investigation of this issue within the Fisher matrix formalism is presented in Ref. [27] for spectroscopic redshift surveys such as BOSS (baryon oscillation spectroscopic survey [28]) or DESI (dark energy spectroscopic instrument [29]), but also including input from the cosmic microwave background (CMB), in particular, Planck [10] and weak gravitational lensing surveys such as DES (Dark Energy Survey [30])

and LSST (Large Synoptic Survey Telescope [31]). A similar analysis for surveys like Euclid [32] can be found in Ref. [33]. The power of purely large-scale measurements, such as baryon acoustic oscillations (BAO) is significantly reduced by the uncertainty in neutrino masses, and employing broadband galaxy power at much smaller scales becomes important in improving our ability to extract information about dark energy as well as the neutrino sector [27].

Due to their large thermal velocities, $v_{\rm th}(z)$, neutrinos do not cluster at scales smaller than the free-streaming scale $k_{\rm FS}(z) \sim H(z)/v_{\rm th}(z)$. For neutrinos turning nonrelativistic in the matter dominated regime, the comoving free-streaming scale has a maximum value at the time when the neutrinos become relativistic. Thus, at length scales larger than those set by this maximum, $k_{\rm nr}$, neutrinos cluster in the same way as dark matter, while at smaller scales their contribution to clustering is much smaller, leading to a suppression of the total matter power spectrum. In linear perturbation theory this suppression increases with increasing wave-number asymptoting to a value of $\sim 8\Omega_\nu/\Omega_{\rm m}$. Since this effect can be observed at length scales too small for linear perturbation theory to hold, it is essential to compute the nonlinear matter power spectrum [34].

The effect of neutrinos at sufficiently large length scales can be studied using perturbation theory; at smaller length scales, matter clustering treated via N-body methods can be used to extend the predictive reach. Moreover, in view of the above discussion, this has to be done in the presence of a varying dark energy equation of state. Our purpose here is to present both perturbative and N-body results for the matter fluctuation power spectrum in the presence of neutrinos and dynamical dark energy. (We do not consider the case of modified gravity here.)

Our results are useful in multiple ways. First, they provide reliable predictions for the matter power spectrum on large scales for ongoing and upcoming BAO measurements like BOSS [28], DESI [29], and CHIME (the Canadian Hydrogen Intensity Mapping Experiment [35]), in particular at higher redshifts. Second, in order to build prediction tools for power spectra well into the nonlinear regime, perturbation theory is very useful to anchor the predictions at high accuracy on large scales. Previously, based on a finite number of cosmological models, we have produced emulators for the power spectrum enabling fast parameter estimation of wCDM cosmologies [36,37]. However, ongoing and future surveys will attempt to go beyond wCDM to constrain both neutrino masses and a time dependent equation of state of dark energy. In preparation for such surveys (see, e.g. Ref. [38]), we use the Hardware/Hybrid Accelerated Cosmology Code (HACC) N-body framework [39–41], extended to include both a time varying dark energy equation of state and an approximate treatment of massive neutrinos, to compute the matter power spectrum. Third, the accurate treatment of neutrinos in N-body simulations is nontrivial as discussed in more detail below. We study the validity of different higher order perturbation theory implementations for a ΛCDM cosmology for which we have high-accuracy simulations. We then use these results to gauge the inaccuracies induced by an approximate treatment of neutrinos in simulations.

Dynamical dark energy can be treated in two different ways. One can either begin with a model, specified by an action, and aim to constrain its parameters. For example, a scalar field quintessence model [42,43] can be written down with a power law potential whose parameters can then be determined by the data. Such models can be subdivided, for example, into "freezing" and "thawing" classes, in which the scalar field moves respectively toward or away from a stationary point in its potential [44]. Canonical scalar fields have pressure-to-energy-density ratios ("equations of state") ranging between -1 and 1, and their sound speeds are equal to the speed of light; however, k-essence models relax both of these restrictions [45].

The second, more phenomenological, approach to dark energy is to parametrize its equation of state and sound speed as functions of time or scale factor. Although an action is necessary for predicting the effects of dark energy across a range of energy and distance scales, a dark energy which does not cluster gravitationally and does not couple to any other particle can really only be constrained on cosmological scales, so such a parametrization is sufficient. Here we adopt the commonly used form [46,47],

$$w(a) = w_0 + w_a(1-a), \tag{1}$$

and we assume a sound speed $c_s^2 = 1$. This representation of $w(a)$ smoothly parametrizes a large range of models including freezing and thawing scalar fields, phantom energy with $w < -1$, and early dark energy. One of its limitations is that constraints on early dark energy imply $w_0 + w_a \lesssim 0$, limiting the rate at which $w(a)$ can change at recent times [48]. However, since the data are not powerful enough to constrain a large number of dark energy parameters, this parametrization is a reasonable compromise, and is used in analyzing the results from many surveys.

B. Perturbation theory and N-body simulations

Over the past several years, higher-order cosmological perturbation theory has been crafted into a useful tool for understanding the growth of large-scale structure. Applying the continuity and Euler equations to an effective matter fluid with an irrotational velocity field, perturbation theory lets us predict the power spectrum of large-scale structure at early times and at moderately nonlinear scales. Although the scale-dependent growth rate in massive neutrino models is incompatible with most perturbative methods, so-called

time renormalization group (Time-RG) perturbation theory accommodates massive neutrinos by directly integrating the evolution equations for the power spectrum [49,50]. In this work we extend the publicly available CPTER perturbation theory code [51,52] to include massive neutrinos and dynamical dark energy. In our perturbative treatment, as well as in our computation of the scale-dependent growth, we treat neutrinos as a linear source for growth of cold dark matter and baryonic density perturbations.

The regime of validity of perturbation theory cannot be calculated rigorously, and at sufficiently small scales the fluid approximation breaks down [53–56]. Currently the most reliable test of perturbation theory is a direct comparison with N-body simulations, which approximate dark matter as a collection of point particles, obtaining dynamical Monte Carlo solutions to the Vlasov-Poisson system of equations. Such a comparison is given in Ref. [51] using a large range of perturbation theory methods for ΛCDM cosmologies, and quantifying the accuracy of each perturbative method. Here we use N-body simulations to test Time-RG and a few other perturbation theories, for models with dynamical dark energy and massive neutrinos, up to redshifts $z = 3$.

While N-body simulations are the accepted way to compute the nonlinear matter power spectrum of cold dark matter, including neutrinos in the simulation as particles is difficult because of their large thermal velocities, and artificial clustering induced by having multiple species of particles with very different particle masses. Consequently, different groups have computed nonlinear corrections to the matter power spectrum due to massive neutrinos by adopting different approaches. Perturbation theory was extended to the quasinonlinear regime by using standard second order perturbation theory in Ref. [57]. In Ref. [58], the authors account for neutrinos in the initial conditions for the CDM particles in the simulations, and add the linearly evolved neutrino fluctuations to the particle fluctuations to obtain the total power spectrum, ignoring the nonlinear interaction of the neutrinos with the dark matter. An alternative approach to studying the effect of neutrinos at small scales by using the halo model is pursued in Ref. [59].

Gravitational interactions between neutrinos and dark matter particles were self-consistently incorporated in Ref. [60] by including neutrino particles in N-body simulations with a thermal velocity sampled from the appropriate Fermi-Dirac distribution in addition to a flow velocity to set up initial conditions, typically starting the (neutrino) simulation at very late times so that the neutrino thermal velocity is relatively small [60–62]. The aim of this was to avoid difficulties of the sort encountered in Ref. [63] and in other earlier simulation efforts.

To extend the treatment further, in Refs. [61,64], the authors propagate a linearly evolved neutrino perturbation on a grid, and CDM particles in an N-body simulation that evolves under the influence of self-gravity as well as the potential sourced by the neutrino fluid on the grid. Further improvements to this method were introduced in Ref. [65] where this approach was combined with a particle representation to study sub-Mpc effects of neutrino clustering, and in Ref. [66] who also evolve the neutrino density in the nonlinear potentials sourced by the CDM particles. These nonlinear corrections show that the nonlinear matter power spectrum is suppressed to a maximum of $\sim 10\Omega_\nu/\Omega_{\rm m}$, (as compared to $\sim 8\Omega_\nu/\Omega_{\rm m}$ found in linear theory mentioned earlier) and the suppression decreases for wave numbers larger than a certain value $k_{\rm turn}$ which depends on the neutrino mass.

Our goal is to calculate the power spectrum in the presence of (i) massive neutrinos and (ii) time-varying dark energy equations of state, only up to $k \approx 0.3h$ Mpc^{-1}, allowing us to simplify the treatment of neutrinos considerably. We include these two new physical ingredients in both simulations and higher-order perturbation theory, finding that the two methods agree at the 2% level up to $k \sim 0.1h$ Mpc^{-1} at $z = 0$, and better at higher redshifts. Through perturbative arguments we show that our simple approximation for neutrinos in the N-body simulations, following Refs. [57,58], is valid at the 1% level over the entire region of applicability of perturbation theory, justifying its use in our code. Finally, we apply our perturbative calculations to determine the effect on the power spectrum of varying neutrino masses and the two dark energy equation of state parameters, finding, for example, that neutrino inhomogeneities have little effect on the BAO scale.

The remainder of this paper is organized as follows. Section II summarizes perturbation theory results, including Time-RG when massive neutrinos are included. Our N-body simulations are described in Sec. III. Tests of perturbation theory with dynamical dark energy and massive neutrinos are conducted in Sec. IV and presented along with discussions of observable effects. The final results are summarized in Sec. V.

II. HIGHER-ORDER PERTURBATION THEORY

A. Standard perturbation theory

Consider a universe containing nonrelativistic, noninteracting matter with density, $\rho_{\rm m}(\vec{x}, t)$, as well as nonclustering dark energy with density $\rho_{\rm de}(t)$ and equation of state parameter w. Under the assumptions of an irrotational velocity field ($\nabla \times \vec{v} = 0$) and no shell crossings, the matter can be described in terms of a density contrast, $\delta(\vec{x}, t) = (\rho_{\rm m} - \bar{\rho}_{\rm m})/\bar{\rho}_{\rm m}$, and a velocity divergence, $\theta(\vec{x}, t) = \nabla \cdot \vec{v}$. In Fourier space, the continuity and Euler equations imply

$$\frac{\partial \delta(\vec{k}, a)}{\partial \log a} = -\frac{\theta(\vec{k}, a)}{aH} - \int \frac{d^3p d^3q}{aH(2\pi)^3} \delta_{\rm D}(\vec{k} - \vec{p} - \vec{q}) \times \frac{\vec{k} \cdot \vec{p}}{p^2} \theta(\vec{p}, a) \delta(\vec{q}, a) \quad (2)$$

$$\frac{\partial\theta(\vec{k},a)}{\partial\log a} = -\theta(\vec{k},a) - \frac{3}{2}\Omega_{\rm m} aH\delta(\vec{k},a) - \int \frac{d^3p d^3q}{aH(2\pi)^3} \times \delta_{\rm D}(\vec{k}-\vec{p}-\vec{q})\frac{k^2(\vec{p}\cdot\vec{q})}{2p^2q^2}\theta(\vec{p},a)\theta(\vec{q},a), \quad (3)$$

where a is the scale factor, defined to be unity today, H is the Hubble parameter, and $\delta_{\rm D}$ is the Dirac delta function. The second term on the right-hand side of Eq. (3) describes gravitational clustering according to the Poisson equation. The final term on the right in each of the above makes the evolution nonlinear. If these two terms are neglected, Eqs. (2)–(3) can be integrated easily. The resulting linear theory describes the Universe on the largest scales. The $\vec{k}$-independent linear growth factor $D(a)$ is the growing-mode solution $\delta_{\rm lin}(\vec{k},a)$ to these linearized equations, also normalized to unity today.

The nonlinear evolution equations Eqs. (2)–(3) can be expressed in a more compact notation. Define the perturbation variables, φ_a, the evolution function matrix, Ω_{ab}, and the vertex functions, γ_{abc}, as

$$\varphi_0(\vec{k},a) = \delta(\vec{k},a)a_{\rm in}/a \quad (4)$$

$$\varphi_1(\vec{k},a) = -\theta(\vec{k},a)a_{\rm in}/(a^2H) \quad (5)$$

$$\Omega_{00} = -\Omega_{01} = 1 \quad (6)$$

$$\Omega_{10}(a) = -\frac{3\Omega_{\rm m}H_0^2}{2a^3H^2} = -\frac{3}{2}\Omega_{\rm m}(a) \quad (7)$$

$$\Omega_{11}(a) = 3 + \frac{d\log H}{d\log a} \quad (8)$$

$$\gamma_{010}(\vec{k},\vec{p},\vec{q}) = \gamma_{001}(\vec{k},\vec{q},\vec{p}) = \delta_{\rm D}(\vec{k}+\vec{p}+\vec{q})(\vec{p}+\vec{q})\cdot\vec{p}/(2p^2) \quad (9)$$

$$\gamma_{111}(\vec{k},\vec{p},\vec{q}) = \delta_{\rm D}(\vec{k}+\vec{p}+\vec{q})(\vec{p}+\vec{q})^2\vec{p}\cdot\vec{q}/(2p^2q^2), \quad (10)$$

where all other γ_{abc} are zero, and $a_{\rm in} \ll 1$ is the initial value of the scale factor, which we assume to be small enough that the evolution is linear. Then the evolution equations (2)–(3) can be written in the form,

$$\frac{\partial\varphi_a(\vec{k},a)}{\partial\log a} = -\Omega_{ab}(a)\varphi_b(\vec{k},a) + \frac{a}{a_{\rm in}}\int\frac{d^3p d^3q}{(2\pi)^3} \times \gamma_{abc}(\vec{k},-\vec{p},-\vec{q})\varphi_b(\vec{p},a)\varphi_c(\vec{q},a), \quad (11)$$

where repeated indices indicate summation.

A thorough description of standard perturbation theory (SPT) is provided in Ref. [51], which we summarize here. Let us begin by assuming an Einstein–de Sitter (EdS) universe, in which $\Omega_{\rm m} = 1$ and there are no species other than cold matter. Equations (6)–(8) imply

$$\Omega = \begin{bmatrix} 1 & -1 \\ -\frac{3}{2} & \frac{3}{2} \end{bmatrix}. \quad (12)$$

Choose $a_{\rm in} \ll 1$ such that perturbations $\delta_{\rm lin}(k,a_{\rm in})$ are linear. Since $D(a) = a$, $\delta_{\rm lin}(k,a) = \delta_{\rm lin}(k,a_{\rm in})a/a_{\rm in}$. SPT expands the solution to the nonlinear evolution equations in powers of the linear density contrast, $\delta(\vec{k},a) = \sum_{n=1}a^n\delta_n(\vec{k})$, where $\delta_n(\vec{k})$ is a mode-coupling integral over the product of n $\delta_{\rm lin}$s, $\delta_n(\vec{k}) = \int d^3p_0\ldots d^3p_{n-1}\delta_{\rm D}\times(\vec{k}-\sum\vec{p}_i)F_n(\vec{p}_0,\ldots,\vec{p}_{n-1})\times\delta_{\rm lin}(\vec{p}_0,a_{\rm in})\ldots\delta_{\rm lin}(\vec{p}_{n-1},a_{\rm in})$, and the F_n are determined by Eqs. (2)–(3) as in Ref. [51]. The matter power spectrum $P(k,a)$ is then

$$\begin{aligned}(2\pi)^3\delta_{\rm D}(\vec{k}+\vec{k}')P(k,a) &= \langle\delta(\vec{k})\delta(\vec{k}')\rangle \\ &= \frac{a^2}{a_{\rm in}^2}\langle\delta_1(\vec{k})\delta_1(\vec{k}')\rangle + 2\frac{a^4}{a_{\rm in}^4}\langle\delta_1(\vec{k})\delta_3(\vec{k}')\rangle \\ &\quad + \frac{a^4}{a_{\rm in}^4}\langle\delta_2(\vec{k})\delta_2(\vec{k}')\rangle + \ldots \\ &= (2\pi)^3\delta_{\rm D}(\vec{k}+\vec{k}')[P_{\rm lin} + P^{(1,3)} + P^{(2,2)} + \ldots], \end{aligned} \quad (13)$$

where $P_{\rm lin}$ is the linear power spectrum, and the next-order ("one-loop") nonlinear corrections are given by [67]

$$P^{(1,3)} = \frac{k^3P_{\rm lin}(k)}{1008\pi^2}\int_0^\infty drP_{\rm lin}(kr)\left[\frac{12}{r^2} - 158 + 100r^2 - 42r^4 + \frac{3(r^2-1)^3(7r^2+2)}{r^2}\ln\left|\frac{1+r}{1-r}\right|\right] \quad (14)$$

$$P^{(2,2)} = \frac{k^3}{392\pi^2}\int_0^\infty drP_{\rm lin}(kr)\int_{-1}^1 dxP_{\rm lin}\left(k\sqrt{1+r^2-2rx}\right) \times\frac{(3r+7x-10rx^2)^2}{(1+r^2-2rx)^2}. \quad (15)$$

Here the dependence $P_{\rm lin}(k,a) = P_{\rm lin}(k,a_{\rm in})a^2/a_{\rm in}^2$ upon a has been suppressed. The above approach can easily be extended to higher-order terms (the two-loop terms) as well as to the velocity power spectrum and the density-velocity cross power spectrum.

B. Scale-independent growth

Now let us consider a universe which has a homogeneous component with arbitrary equation of state in addition to CDM and baryonic matter, resulting in a scale-independent growth factor $D(a)$. This homogeneous

component may include a nonclustering dark energy as well as a radiation component whose energy density is small enough that its clustering may be neglected. If we make the replacement $\varphi_1 \to \varphi_1/f$ with $f = d\log D/d\log a$, and we change the time variable in Eq. (11) from $\log a$ to $\log[D(a)/D(a_{\rm in})]$, then the evolution matrix becomes

$$\Omega = \begin{bmatrix} 1 & -1 \\ \frac{3\Omega_{\rm m}(a)}{2f^2} & \frac{3\Omega_{\rm m}(a)}{2f^2} \end{bmatrix}. \tag{16}$$

If the equation of state parameter does not differ too much from -1, then to reasonable precision, $f(a) \approx \Omega_{\rm m}(a)^{0.55}$ [68]. It follows that $\Omega_{\rm m}(a)/f(a)^2 \approx \Omega_{\rm m}^{-1/10}$, which can itself be approximated as unity at the $\approx$10% level for $\Omega_{\rm m}(a) \geq 0.3$, and the evolution matrix can be approximated by its EdS counterpart (12). As a result, the $P^{(1,3)}$ and $P^{(2,2)}$ corrections are given by Eqs. (14), (15), the only difference being the dependence of $P_{\rm lin}(k,a) = P_{\rm lin}(k,a_{\rm in})D(a)^2/D(a_{\rm in})^2$ upon a.

C. Massive neutrinos and Time-RG

Massive neutrinos cluster like cold matter on large scales but free-stream out of bound structures on small scales. Moreover, since their velocities redshift away as the universe expands, the free-streaming length scale changes with time. Thus the growth factor depends on the wave number k as well as a, and the method used in Sec. II B to determine the 1-loop terms from their EdS counterparts breaks down. (Rapidly evolving dark energy models [69] as well as scale-dependent fifth forces from modified gravity are also inconsistent with the method of Sec. II B.) Scale-dependent growth introduces a k dependence into Ω_{10}, the source term of the Poisson equation, since CDM and neutrinos cluster differently on different scales.

Time-renormalization group perturbation theory generalizes Eq. (11) to $\vec{k}$-dependent Ω and integrates directly to find the power spectrum [49]. Since Eqs. (2), (3) relate the time-derivative of the first-order perturbations δ and θ to second-order terms, there is an infinite tower of evolution equations for the power spectra,

$$\frac{\partial\langle\varphi_a\varphi_b\rangle}{\partial\log a} = -\Omega_{ac}\langle\varphi_c\varphi_b\rangle - \Omega_{bc}\langle\varphi_a\varphi_c\rangle + \frac{a}{a_{\rm in}}\gamma_{acd}\langle\varphi_c\varphi_d\varphi_b\rangle + \frac{a}{a_{\rm in}}\gamma_{bcd}\langle\varphi_a\varphi_c\varphi_d\rangle \tag{17}$$

$$\frac{\partial\langle\varphi_a\varphi_b\varphi_c\rangle}{\partial\log a} = -\Omega_{ad}\langle\varphi_d\varphi_b\varphi_c\rangle - \Omega_{bd}\langle\varphi_a\varphi_d\varphi_c\rangle - \Omega_{cd}\langle\varphi_a\varphi_b\varphi_d\rangle + \frac{a\gamma_{ade}}{a_{\rm in}}\langle\varphi_d\varphi_e\varphi_b\varphi_c\rangle + \frac{a\gamma_{bde}}{a_{\rm in}}\langle\varphi_a\varphi_d\varphi_e\varphi_c\rangle + \frac{a\gamma_{cde}}{a_{\rm in}}\langle\varphi_a\varphi_b\varphi_d\varphi_e\rangle, \tag{18}$$

and so on, each equation relating the evolution of the n-point correlation functions to the $(n+1)$-point correlation functions. In this formalism, linear theory corresponds to setting to zero the bispectrum $\delta_{\rm D}(\vec{k}+\vec{p}+\vec{q})B_{abc}(\vec{k},\vec{p},\vec{q},a)$, truncating this tower after Eq. (17). Time-RG uses the next level of approximation, allowing nonzero B_{abc} but setting to zero the trispectrum, the connected part of the four-point correlation function. Direct integration of the $\vec{k}$-dependent evolution equations (17), (18) means that the assumptions of scale-independent growth and a time-independent evolution matrix are no longer necessary.

Consider a universe with two matter fluids, a cold fluid representing CDM and baryons as well as a warm fluid representing neutrinos. From now on let φ_0 and φ_1 in Eqs. (4), (5) refer to density and velocity divergence perturbations in the cold fluid alone, denoted by the subscript cb. Since neutrinos do not cluster on small scales, they are well-described by the linearized evolution equations. Their density contrast $\delta_{\nu,\rm lin}(k,a)$ can be found using a linear Boltzmann code such as CAMB [70], based on CMBFAST [71–73]. Then Ω_{10}, the source term for the CDM and baryon velocity divergence, is given by

$$\Omega_{10}(k,a) = -\frac{3}{2}\Omega_{\rm m}(a)\left[f_{\rm cb} + f_\nu\frac{\delta_{\nu,\rm lin}(k,a)}{\delta_{\rm cb,lin}(k,a)}\right], \tag{19}$$

where $f_{\rm cb} = \Omega_{\rm cb}/\Omega_{\rm m}$ and $f_\nu = \Omega_\nu/\Omega_{\rm m}$ are evaluated today. Note that Ω_{10} uses the linear cb density contrast rather than the nonlinear one; Ref. [50] shows that this approximation introduces an error of only $\approx$0.1%.

Time-RG perturbation theory directly integrates the evolution equations (17), (18) with the evolution matrix given by Eqs. (6), (8), (19) and vertices given by Eqs. (9), (10). Initial conditions are given by $\langle\varphi_a\varphi_b\rangle = P_{\rm lin}f^{a+b}$ and $\langle\varphi_a\varphi_b\varphi_c\rangle = 0$ evaluated at $a_{\rm in}$ sufficiently small that the perturbations are linear. Calculations presented here use a modified version of the CPTER code [51,52] in which (i) the homogeneous evolution includes massive neutrinos and dynamical dark energy, and (ii) the linear perturbations are interpolated from CAMB outputs.

III. N-BODY SIMULATIONS

A. Simulations with HACC

In order to test the validity of the perturbation theory approach we run a set of N-body simulations with the HACC framework [39–41]. HACC is a flexible N-body code designed to exploit the diverse landscape of current and future supercomputing architectures. HACC's design is centered around the idea of breaking up the problem into long-range and short-range force evaluations, keeping a highly optimized FFT-based long-range solver the same on all architectures, while optimizing the short-range solver for a specific target architecture. For hardware-accelerated systems, such as those with graphics processing units

TABLE I. Parameters for the models investigated in this paper, where we use $\omega_\nu = \Sigma m_\nu/94$ eV.

#	L $[h^{-1}$ Mpc]	ω_{cdm}	ω_b	ω_ν	n_s	σ_8	h	w_0	w_a	Σm_ν [eV]	PM	High-res
M000n0	1491.0	0.1109	0.02258	0.0	0.9630	0.8000	0.7100	−1.0	0.0	0.0	16	1
M000n1	1491.0	0.1009	0.02258	0.010	0.9630	0.8000	0.7100	−1.0	0.0	0.94	16	1
M000n2	1491.0	0.1099	0.02258	0.001	0.9630	0.8000	0.7100	−1.0	0.0	0.094	16	0
M001n0	1295.1	0.1246	0.02261	0.0	0.9611	0.8778	0.6167	−0.7	0.6722	0.0	16	1
M001n1	1295.1	0.1216	0.02261	0.003	0.9611	0.8778	0.6167	−0.7	0.6722	0.282	16	0
M002n1	1224.9	0.0981	0.02283	0.003	0.8722	0.7789	0.5833	−1.167	1.15	0.282	16	0

(GPUs), particle-particle particle mesh (P^3M) solvers can be easily optimized, while TreePM methods are better suited for nonaccelerated systems. HACC has been shown to scale to the largest machines currently available. The results shown in this paper have been obtained on the Blue Gene systems Intrepid (BG/P) and Mira (BG/Q) at Argonne National Laboratory and on Titan, a GPU-accelerated system at Oak Ridge National Laboratory.

We ran a suite of N-body simulations covering different cosmological models as summarized in Table I. Our investigations in Sec. IV start with a ΛCDM model (M000) to set a well-tested baseline for studying the range of validity of the different perturbation theories. For this model we analyze one high-resolution simulation, evolving 3200^3 particles in a $(2100\ \text{Mpc})^3$ volume with a force resolution of 6.6 kpc. The starting redshift of the simulation is $z_{\text{in}} = 200$ and the Zel'dovich approximation [74] is used to set up the initial conditions. In order to obtain good statistics on large scales, we also carry out a set of sixteen particle-mesh (PM) simulations, evolving 512^3 particles on a 1024^3 uniform grid. We use the high-resolution simulation to check that the PM simulations yield accurate results up to the scales we are testing the different perturbation theory approaches. As detailed in Table I we have high-resolution simulations for three of the models, the ΛCDM model with and without massive neutrinos and one model with a time varying dark energy equation of state (all three simulations evolving 3200^3

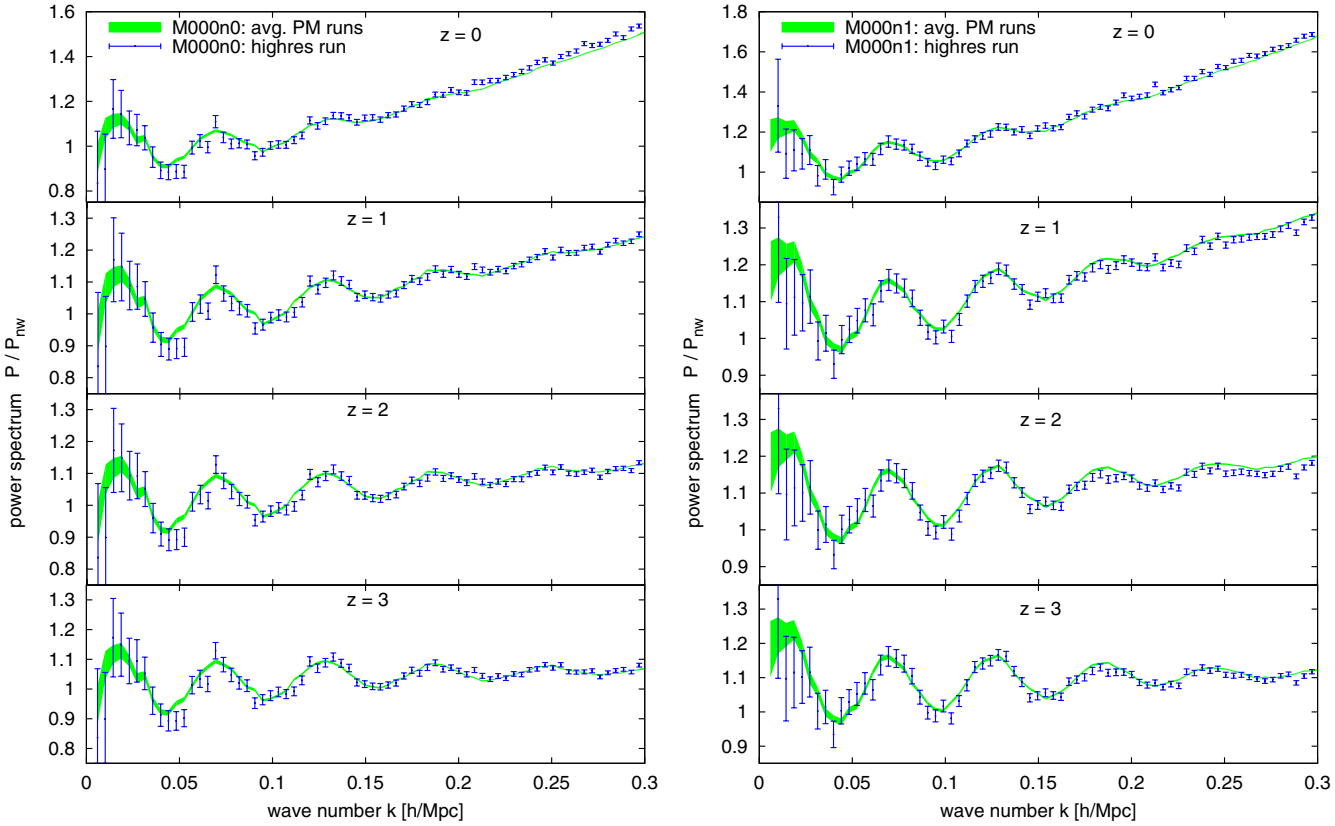

FIG. 1 (color online). Comparison between the average of 16 PM realizations (green band) and a high resolution simulation (blue points). The agreement is very good up to $k \approx 0.3\ h$ Mpc^{-1} over the redshift range of interest. The left panel shows model M000n0 (ΛCDM) and the right panel, M000n1 (ΛCDM with massive neutrinos) of Table I, both divided by the no-wiggle power spectrum of Eq. (29).

particles in a $(2100\ \mathrm{Mpc})^3$ volume). For all models we generate sixteen PM runs with the same specifications as given above. Figure 1 shows the comparison of the high-resolution simulations with and without neutrinos with the average power spectrum from the PM simulations. The agreement is very good out to $k \sim 0.3h\ \mathrm{Mpc}^{-1}$, the maximum value for which we compare our results with higher order perturbation theory results presented in the next section.

In order to carry out simulations beyond wCDM models, we implement some new features into HACC, namely a time varying equation of state parametrized by (w_0, w_a) via Eq. (1), as well as the addition of massive neutrinos. As described in more detail below, we treat neutrinos in an approximate way—the perturbative results can be used to estimate how well the approximations work, at least on large and quasinonlinear scales. In the following, we provide a brief description of our neutrino and dynamical dark energy implementations within HACC.

B. Neutrino treatment and dynamical dark energy

The impact of dynamical dark energy and neutrinos on the simulated matter power spectrum are taken into account by (i) modifying the initializer and (ii) including both effects in the background evolution. We do not model the interactions of massive neutrino fluctuations with the dissipationless matter fluctuations during the simulations, i.e., we run HACC as a gravity-only code with a single species representing the sum of CDM and baryons. The total matter power spectrum is constructed from the nonlinear CDM + baryon power spectrum and the (linear) massive neutrino power spectrum from CAMB at the redshift of interest,

$$P(k,a) = \left[f_{\mathrm{cb}}\sqrt{P_{\mathrm{cb}}(k,a)} + f_\nu\sqrt{P_\nu(k,a)}\right]^2. \tag{20}$$

This approach is reasonable since neutrinos do not cluster strongly on small scales, and has been adopted in previous numerical work, see, e.g., Ref. [58], as well as in perturbation theory [57].

In order to set up initial conditions for the HACC simulations we first determine the shape and normalization of the total power spectrum at $a = 1$ $(z = 0)$ using linear theory,

$$P_{\mathrm{total}}(k, a=1) = \mathrm{A}k^{n_s}T^2_{\mathrm{total}}(k, a=1), \tag{21}$$

with n_s being the primordial spectral index,

$$T_{\mathrm{total}}(k, a=1) = f_{\mathrm{cb}}T_{\mathrm{cb}}(k, a=1) + f_\nu T_\nu(k, a=1), \tag{22}$$

$$T_{\mathrm{cb}}(k, a=1) = f_{\mathrm{b}}T_{\mathrm{b}}(k, a=1) + f_{\mathrm{CDM}}T_{\mathrm{CDM}}(k, a=1), \tag{23}$$

and using an associated σ_8 normalization at $z = 0$ which implicitly defines the value of the amplitude coefficient, A. A scale-independent CDM-like growth function, $D(a)$, is then used to move the P_{cb} piece of the power spectrum back to the initial redshift, z_i, and to set the initial particle positions and velocities for our single species code representing both CDM and baryons. This growth function takes into account all species in the homogeneous background which makes comparison to high redshift linear theory outputs from CAMB more direct; radiationlike terms are kept because they change the amplitude by several percent at $z \sim 100$. It does not, however, take into account the scale dependence that neutrinos and baryons would contribute, therefore our terminology "CDM-like."

Our homogeneous background definitions assume that massive neutrinos, if present, are massive enough to be matterlike at $z = 0$. The following equations are written for both massless and massive neutrinos, though only one or the other may be present, not both,

$$\Omega_r = \frac{2.471\times10^{-5}}{h^2}\left(\frac{T_{\mathrm{CMB}}}{2.725^{\circ}\mathrm{K}}\right)^4, \tag{24}$$

$$f^{\mathrm{massless}}_{\nu,r} = \frac{7}{8}\left(\frac{4}{11}\right)^{4/3}N^{\mathrm{massless}}_{\mathrm{eff}}, \tag{25}$$

$$f^{\mathrm{massive}}_{\nu,r} = \frac{7}{8}\left(\frac{4}{11}\right)^{4/3}N^{\mathrm{massive}}_{\mathrm{eff}}, \tag{26}$$

$$\Omega_\nu(a) = \max(\Omega_\nu a^{-3}, f^{\mathrm{massive}}_{\nu,r}\Omega_r a^{-4}), \tag{27}$$

$$\begin{aligned} H^2(a)/H_0^2 = {} & \Omega_{cb}a^{-3} + (1 + f^{\mathrm{massless}}_{\nu,r})\Omega_r a^{-4} + \Omega_\nu(a) \\ & + [1 - \Omega_m - (1 + f^{\mathrm{massless}}_{\nu,r})\Omega_r] \\ & \times a^{-3(1+w_0+w_a)}\exp[-3w_a(1-a)]. \end{aligned} \tag{28}$$

The scale independent CDM-like growth function is the linear equivalent of the (nonlinear) gravity-only operator in HACC that uses the equivalent definitions of the homogenous background as in Eq. (28).

The approximations used to incorporate the effects of baryons and massive neutrinos are similar in that each has a scale-dependent growth and would impart scale dependence in the CDM growth. The shapes and amplitudes are also defined in terms of the linear power spectra, and the goal is to produce accurate power spectra at low redshifts with nonlinear clustering effects in the CDM and baryons. The approximations for baryons and massive neutrinos differ in that the mass of baryons is deposited on the dissipationless gravitationally interacting particles advanced by HACC, but the massive neutrinos are only accounted for with linear theory, as described above.

We would like to stress that using the total power spectrum from CAMB directly at the initial redshift to initialize the particle positions and velocities would lead to

inconsistent results in a gravity-only N-body code: CAMB accounts for baryon-photon coupling and the scale dependence in the growth function which are absent in the N-body code.

In order to account for the presence of dynamical dark energy we modify CAMB as follows. For including dynamical dark energy, we need to (i) modify the equations describing the evolution of the background which results in a change of the perturbations of dark matter, radiation and neutrinos and (ii) modify the equations describing the density and velocity perturbations in the dark energy. The modification to the background cosmology is trivially achieved by modifying the equation describing the evolution of conformal time as a function of the scale factor, using the evolution of dark energy density [see Eq. (28)]. Modifying the equations describing the perturbations of dark energy requires an expression for the speed of sound. Consistent with a simple scalar field model, we assume that this is the speed of light. As a result, perturbations of dark energy develop only on the Hubble scale. A second issue is that the equations describing the evolution of the velocity perturbations include terms of the form $c_s^2/(1+w(a))$, where c_s is the speed of sound in the rest frame of dark energy. For those values of (w_0, w_a) for which the equation of state passes through -1, this results in a singularity. Assuming that at the crossing, this term is small enough that the microscopic properties of dark energy do not modify the power spectra, we replace the term in a small range around the crossing by linearly interpolating between the values at the end of the range, where this term is finite.

IV. RESULTS AND DISCUSSION

A. The regime of validity of perturbation theory

In general, the convergence properties of perturbation theories for the evolution of matter fluctuations cannot be rigorously calculated. Furthermore, at sufficiently nonlinear scales, the fluid approximation to the Vlasov-Poisson equation itself breaks down [53–56]. In the absence of a reliable internal test, the best determination of the accuracy of higher-order perturbative methods is direct comparison against N-body simulations. Since the scales of interest here are large enough that baryonic effects on the growth are small, and sufficient force and mass resolution can be easily attained, predictions for the power spectrum can be controlled to accuracies of better than a percent by using N-body methods (see, e.g. Ref. [75]).

We begin by testing our perturbative calculation for a cosmology with constant dark energy equation of state and massless neutrinos. For this purpose, we use the cosmic emulator of Ref. [36], which uses Gaussian process modeling to interpolate the results of 37 high-resolution N-body simulations chosen to span the cosmological model parameter space. (Previous comparisons of the emulator and perturbation theory can be found in Refs. [55,76].) Figure 2 compares linear perturbation theory, one-loop SPT, and Time-RG to the power spectrum emulator, which is accurate to 1% for $z < 1$ and $k < 1\,h$ Mpc^{-1}. (Full two-loop SPT is sufficiently time-consuming that a similar calculation would be difficult.) As expected, one-loop SPT performs significantly better than linear perturbation theory, especially at high z. Time-RG, which includes some two-loop terms, is even more accurate.

In order to improve the accuracy of the power spectrum computation and to test perturbation theory for models with $w_a \neq 0$, we run high-resolution N-body simulations, shown in Table I. Model M000n0 is a standard ΛCDM model, while M001n0 is an early dark energy model in which $w(z)$ evolves rapidly, allowing the dark energy to be a substantial fraction of the total energy density at the time of recombination. Figure 3 compares linear theory, Time-RG, standard perturbation theory (SPT), renormalized perturbation theory (RPT), and Lagrangian resummation perturbation theory (LPT) to the HACC N-body power spectrum for ΛCDM and early dark energy. RPT is a resummed alternative to the SPT discussed earlier. LPT is formulated in terms of particle displacements, making it particularly useful for observations in redshift space.

In order to present the results more clearly, we have divided the power spectra by a smoothed "no-wiggle" power spectrum $P_{\rm nw}(k,z)$:

$$\frac{1}{P_{\rm nw}(k,0)^{\mu}} = \frac{1}{[(\frac{k}{k_0})^{n_s-\epsilon}P_0]^{\mu}} + \frac{1}{[(\frac{k}{k_1})^{n_s-3}P_1]^{\mu}}, \qquad (29)$$

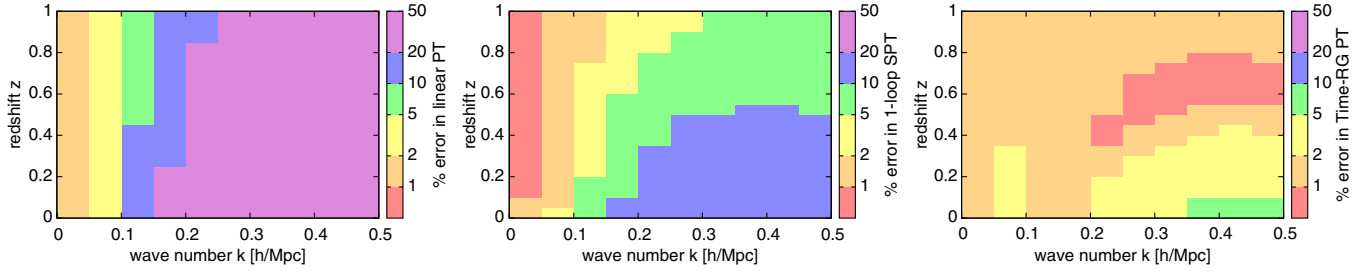

FIG. 2 (color online). Comparison of linear perturbation theory (left), one-loop SPT (middle) and Time-RG (right) to the cosmic emulator of Ref. [36] for dark energy with constant $w = -1.2$ and massless neutrinos. The color of each bin corresponds to the maximum difference between perturbation theory and the emulator power spectrum.

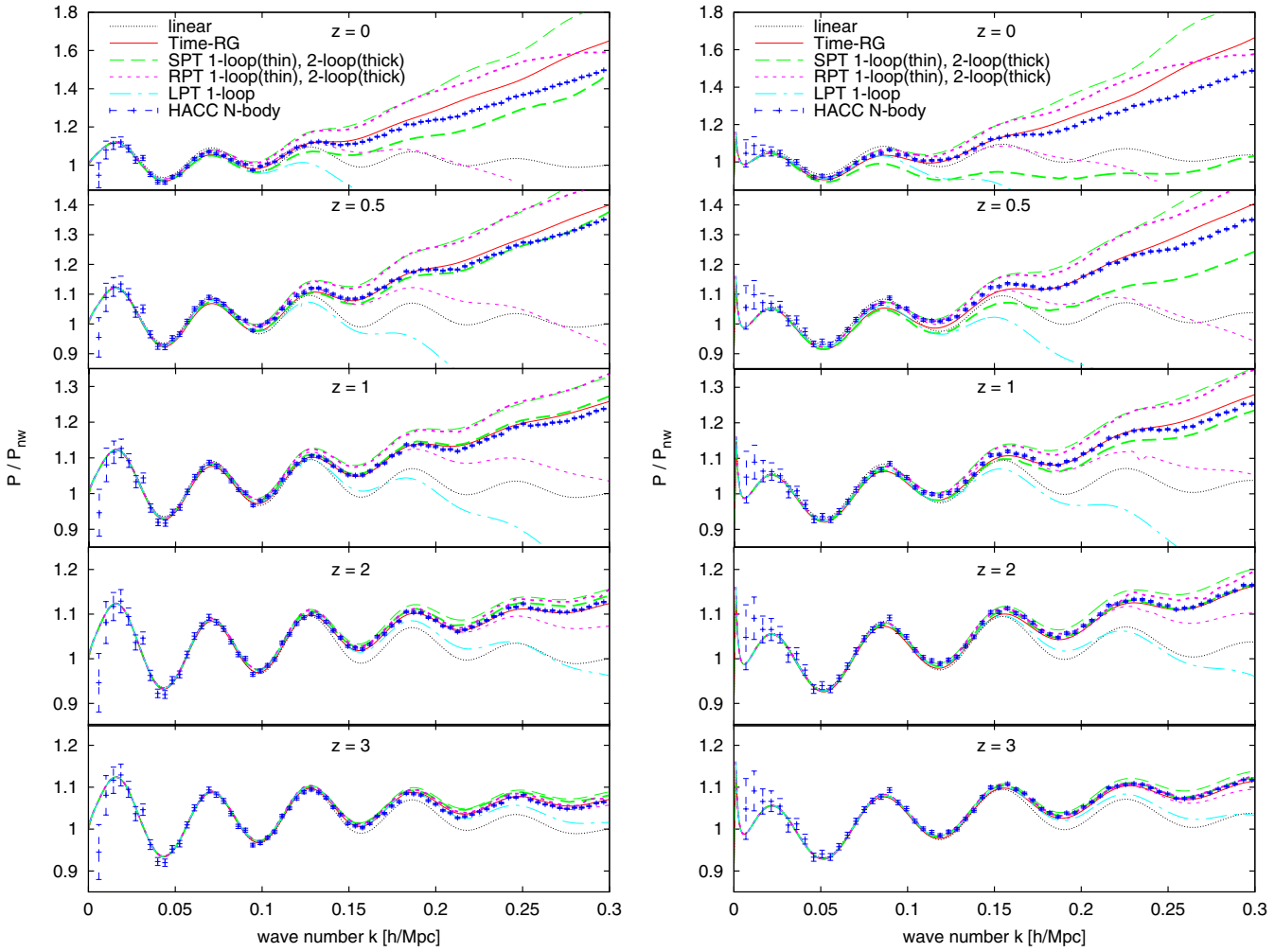

FIG. 3 (color online). Power spectrum ratios for linear theory and four different higher-order perturbation theories compared with the HACC N-body power spectrum at 5 redshifts for models with massless neutrinos. For SPT and RPT, thin and thick lines denote one-loop and two-loop calculations, respectively. Left: ΛCDM, model M000n0. Right: Early dark energy, model M001n0. The wave numbers at which the perturbation theory results deviate from the simulations by 1% and 2% are shown in Table II.

$$P_{\rm nw}(k,z) = D(z)^2 P_{\rm nw}(k,0). \tag{30}$$

Here $k_0 = 10^{-4}h$ Mpc^{-1}, $k_1 = 0.3h$ Mpc^{-1}, $\mu = 0.4$, and we have chosen P_0 and P_1 such that $P_{\rm nw}(k_0)/P_{\rm lin}(k_0) \approx P_{\rm nw}(k_1)/P_{\rm lin}(k_0) \approx 1$. We choose $\epsilon = 0$ except for early dark energy models (we used $\epsilon = 0.2$ for models M001n0 and M001n1; $\epsilon = 0.04$ for M002n1), in which dark energy is a significant fraction ∼10% of the total energy density even at $z \sim 1000$, and the universe is never completely

TABLE II. Wave number k [h Mpc^{-1}] below which each perturbation theory is accurate to 1% (or 2%) in models with massless neutrinos.

				SPT		RPT			
Model	z	Acc.	Linear	one-loop	two-loop	one-loop	two-loop	Time-RG	LPT
M000n0	0	1%	0.076	0.084	0.093	0.14	0.084	0.15	0.093
		2%	0.1	0.11	0.1	0.15	0.11	0.19	0.1
	1	1%	0.13	0.12	0.24	0.2	0.13	0.28	0.14
		2%	0.14	0.15	0.3	0.21	0.17	0.97	0.15
M001n0	0	1%	0.078	0.11	0.058	0.15	0.11	0.17	0.087
		2%	0.078	0.11	0.068	0.15	0.13	0.18	0.097
	1	1%	0.12	0.14	0.16	0.19	0.16	0.26	0.14
		2%	0.16	0.17	0.29	0.2	0.19	0.32	0.15

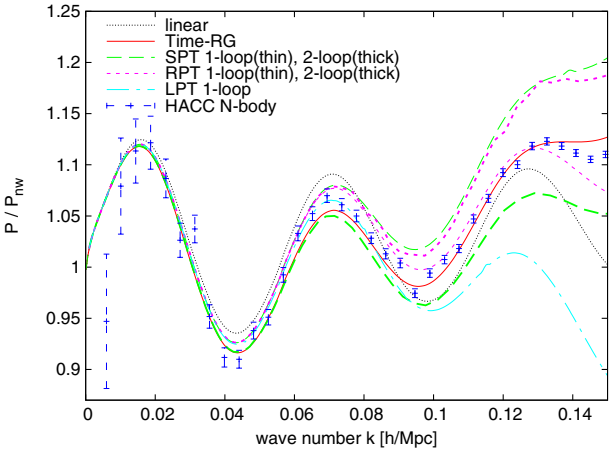

FIG. 4 (color online). Power spectra at $z = 0$ for the M000n0 model from Fig. 3, showing nonlinear suppression of power at intermediate scales.

matter-dominated. $D(z)$ is the scale-independent growth factor found by setting $\delta_\nu = 0$ in Eq. (19).

Figure 3 (left) extends the result of Ref. [51] to higher redshifts, while Fig. 3 (right) is a new result. Table II summarizes the results, showing the k at which each perturbation theory begins to differ from simulations by 1% or 2%. Since the simulated power spectra are noisy at low k, in practice we added the 1% or 2% errors to the 3σ statistical uncertainty of the N-body power spectra.

From Fig. 4 we see that higher-order perturbation theories correctly predict the power spectrum falling below linear theory in the range $0.05h$ Mpc$^{-1} \lesssim k \lesssim 0.1h$ Mpc^{-1} as power moves from large scales to small scales. RPT and one-loop SPT predict the smallest dip, and Time-RG and two-loop SPT predict the largest, while the N-body simulations prefer an intermediate value. In the range $0.1h$ Mpc$^{-1} \lesssim k \lesssim 0.15h$ Mpc^{-1}, Time-RG and one-loop

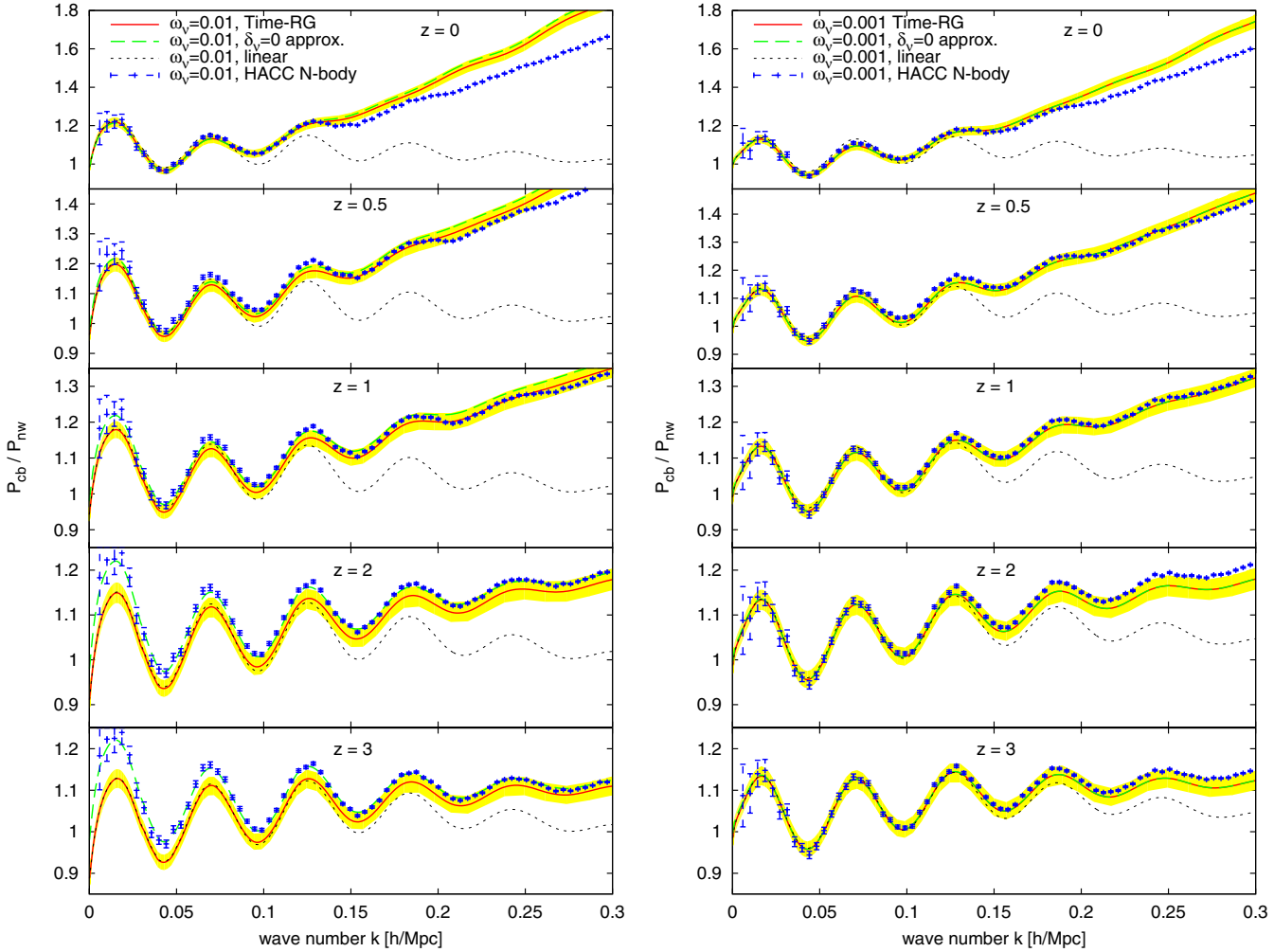

FIG. 5 (color online). Power spectra $P_{\rm cb}$ for models M000n1 (left) and M000n2 (right), with a cosmological constant and massive neutrinos. $P_{\rm nw}$ is the no-wiggle power spectrum of Eq. (29) associated with the linear power spectrum at $z = 0$ in each case. Shaded yellow regions show power spectra within 2% of the corresponding Time-RG curves. Power spectra are also shown with the neutrino density contrast δ_ν set to zero (green dashed curves), the approximation used in the HACC simulations. See the text for further discussion.

RPT most closely approximate the simulations, while SPT and LPT begin to diverge from the other power spectra. At the 2% level, all of the higher-order perturbative methods are accurate up to $k \approx 0.1h$ Mpc^{-1} at $z = 0$.

In the models above, the N-body simulations (and therefore the emulator results based on them) include all gravity effects consistently. When neutrinos are added, this is no longer the case; as discussed earlier, the gravitational potential of clustering of massive neutrinos is not included in the simulations, as this effect is expected to be small. However, a finite neutrino mass leads to a suppression of the power spectrum, and therefore pushes the onset of nonlinear effects to higher wave numbers. Thus, for cosmological models obtained by changing a fraction of the dark matter energy density to the energy density of massive neutrinos (at the same low-k amplitude), perturbation theory must continue to be valid in at least the regime obtained above. Since Time-RG consistently includes the massive neutrinos, we can use it to test the extensions of HACC for massive neutrinos.

B. Massive neutrinos: Perturbation theory and HACC simulations

We now consider cosmological models with massive neutrinos. Since Time-RG is the only perturbative method we consider that includes neutrino masses, all perturbative calculations described below are restricted to Time-RG. Figure 5 shows the power spectra of models M000n1 and M000n2, both of which have cosmological constants and massive neutrinos. The yellow shaded band around the Time-RG curve identifies power spectra within 2% of Time-RG. When ω_ν is small as in Fig. 5 (right), Time-RG agrees with the HACC results to 2% for $k \approx 0.2h$ Mpc^{-1} at $z = 0$ and for even higher k at $z \geq 0.5$. Since Fig. 5 (right) corresponds to $\Sigma m_\nu = 0.094$ eV, about half of the current upper bound, we expect Time-RG to be a good approximation in the most interesting region of parameter space.

The results of Fig. 5 (left) for model M000n1, in which $\omega_\nu = 0.01$ implies a significant neutrino fraction $f_\nu = 7.5\%$ and mass $\Sigma m_\nu = 0.94$ eV, show a discrepancy

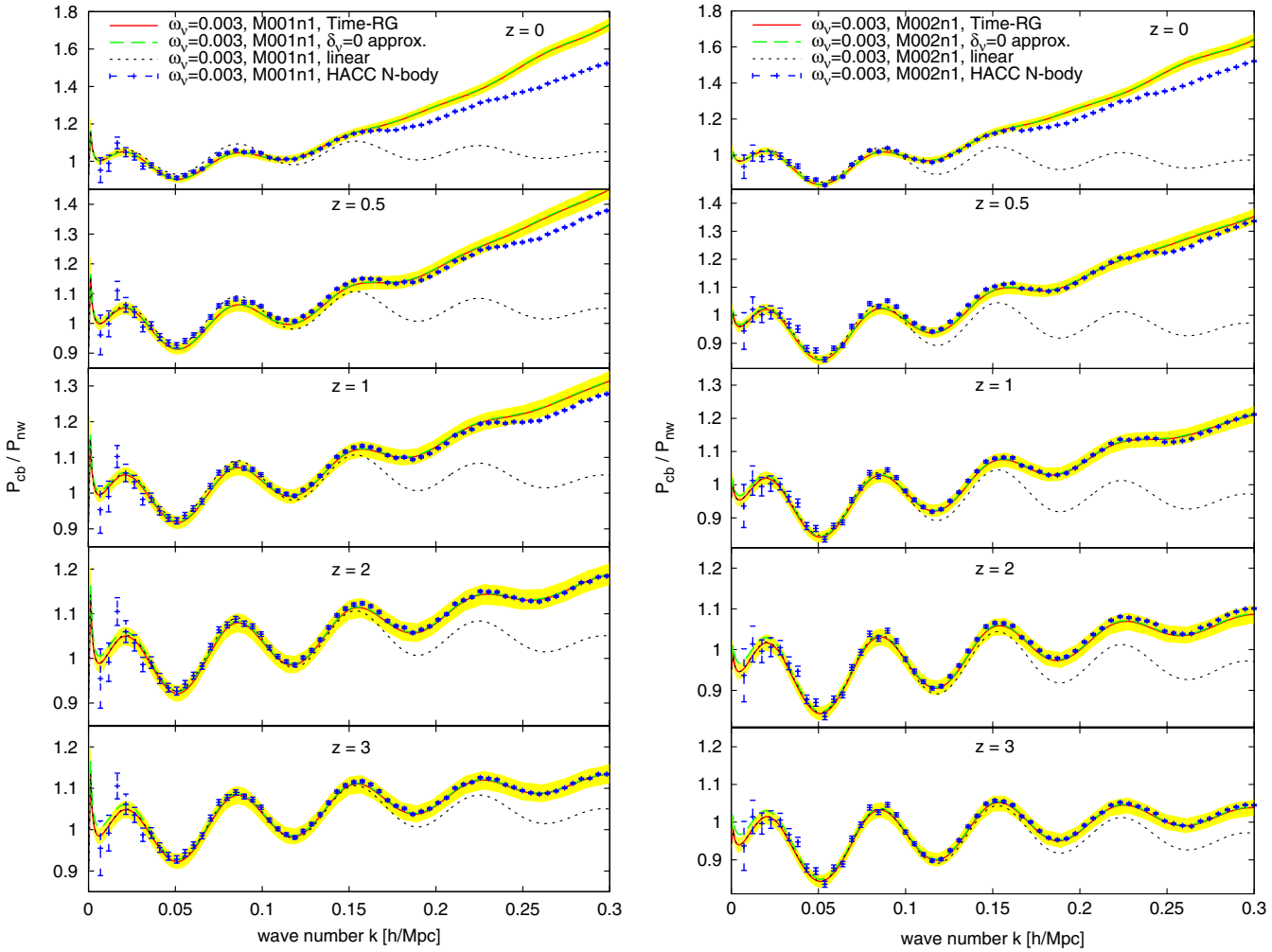

FIG. 6 (color online). Power spectra $P_{\rm cb}$ for the early dark energy models with massive neutrinos, M001n1 (left) and M002n1 (right), following the conventions of Fig. 5.

between Time-RG and the approximate treatment implemented in HACC even for $k < 0.1h$ Mpc^{-1} for the higher-z cases considered. Because the approximation does not include neutrinos as a source for CDM + baryon growth, it is expected to misestimate the power at large f_ν. Note, however, that the neutrino mass implied by this model is about four times as high as the bound from [10].

At $z = 0$, the N-body and perturbative results are normalized correctly by construction, agreeing well at the lowest k values. However, at higher z, the Time-RG curve (red line) should be above the N-body curve (blue points) because the additional neutrino sourcing implies a larger growth function, and hence smaller power spectrum at higher z after normalizing to σ_8 at $z = 0$. In order to display this effect and to estimate its magnitude, we also carried out the Time-RG calculation with $\delta_{\nu,\mathrm{lin}}$ set to zero in Eq. (19), as shown in the long-dashed green curve in Fig. 5 (left). This $\delta_\nu = 0$ curve is in very good agreement with the approximate HACC power spectrum in the low-k regime at all redshifts, showing explicitly that the discrepancy between the Time-RG and HACC results is due to the approximate treatment of neutrinos discussed in Sec. III. (Compensation for this error at the linear level is possible, but we do not pursue it here.) Moreover, a comparison between the Time-RG and $\delta_\nu = 0$ curves provides an estimate of the accuracy of this approximation, which is better than 1% for $z = 0$ up to $k = 0.16h$ Mpc^{-1} and better than 1.5% up to $k = 0.27h$ Mpc^{-1} (although at this point, Time-RG is clearly wrong). This applies to $\omega_\nu = 0.01$, so the error will be several times smaller for lower ω_ν.

Finally, Fig. 6 shows power spectra for two different early dark energy models with massive neutrinos. For both models, Time-RG works quite well, agreeing to mostly better than 2% with the N-body results up to $k = 0.17h$ Mpc^{-1} at $z = 0$.

One possible application of our perturbative results is to combine them with N-body simulations in order to obtain an accurate power spectrum calculation over the greatest possible range of scales. Higher-order perturbation theories such as Time-RG are accurate up to $k = 0.05$–$0.1h$ Mpc^{-1}, as we have confirmed over a large range of dark energy equations of state and neutrino masses. These large scales are precisely where simulations can have some difficulties due to their finite box sizes. Thus by combining Time-RG calculations with those of HACC, it is possible to predict the power spectrum from horizon scales to $k \gtrsim 1h$ Mpc^{-1}.

C. Impact on observables: Exploring physics beyond wCDM using perturbation theory

1. Dynamical dark energy

Growth of structure depends on the dark energy equation of state. In the linear regime the dominant effect will be a scale-independent change to the growth factor $D(a)$. Since we normalize power spectra using σ_8 at $z = 0$, this effect will be most noticeable at higher redshifts. Meanwhile, nonlinearities may introduce a scale-dependent change at larger k.

Figure 7 shows the effects on the power spectrum of varying the equation of state parameters w_0 and w_a, starting from the ΛCDM fiducial model M000n0 from Table I. Power spectra are calculated using the Time-RG perturbation theory; we have divided the power spectra by a smoothed "no-wiggle" power spectrum $P_{\mathrm{nw}}(k)$ specified in Eq. (29).

Our expectation based on linear theory, that changing the equation of state mainly affects $P(k)$ through the growth factor, is essentially correct for w_0. The different curves in Fig. 7 (top panel) differ mostly by a normalization factor, corresponding to the square of the growth factor at $z = 1$. On the other hand, changing w_a appears, from Fig. 7 (bottom panel), to have a greater effect at more nonlinear scales. This is encouraging, as it indicates that the nonlinear power spectrum can provide more powerful constraints on w_a than expected from linear theory.

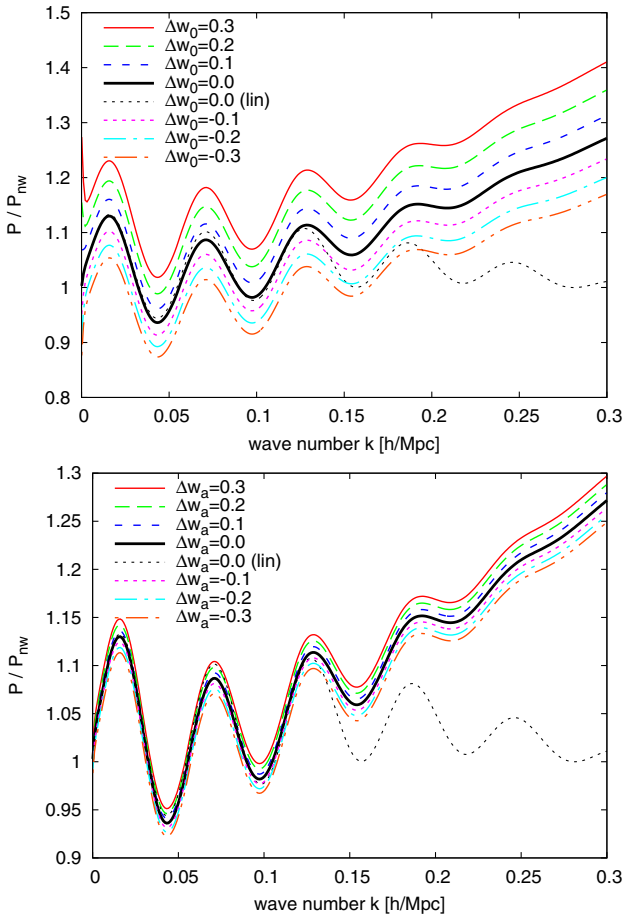

FIG. 7 (color online). Effects of varying w_0 (top) and w_a (bottom) on the Time-RG matter power spectrum $P(k)$ at $z = 1$. The fiducial model $\Delta w_0, \Delta w_a = 0$ is M000n0 in Table I. $P(k)$ has been divided by the no-wiggle power spectrum (29) for clarity.

2. Massive neutrinos

Figure 8 (top panel) begins with model M000n0 and increments ω_ν in steps of 0.002, with $\omega_\nu = 0.01$ corresponding to model M000n1. As for the simulations, the total matter power spectrum $P(k)$ is found by adding the nonlinear CDM and baryon power spectrum to the linear neutrino power spectrum [see Eq. (20)]. Increasing the neutrino mass modifies the power spectrum in a scale-dependent way. We note that all of the models in Fig. 8 (top panel) are normalized to the same σ_8 at $z = 0$. Since neutrinos suppress small-scale power, normalization increases the large-scale power of massive neutrino models to compensate. The bottom panel of Fig. 8 shows the results if one fixes the normalization by adopting the same low-k amplitude in all cases, at some chosen value of k. In this case, the suppression of power due to massive neutrinos is immediately evident. Figure 9 presents the effects of varying ω_ν, as well as w_0 and w_a, using a ratio relative to the minimal ΛCDM model M000n0.

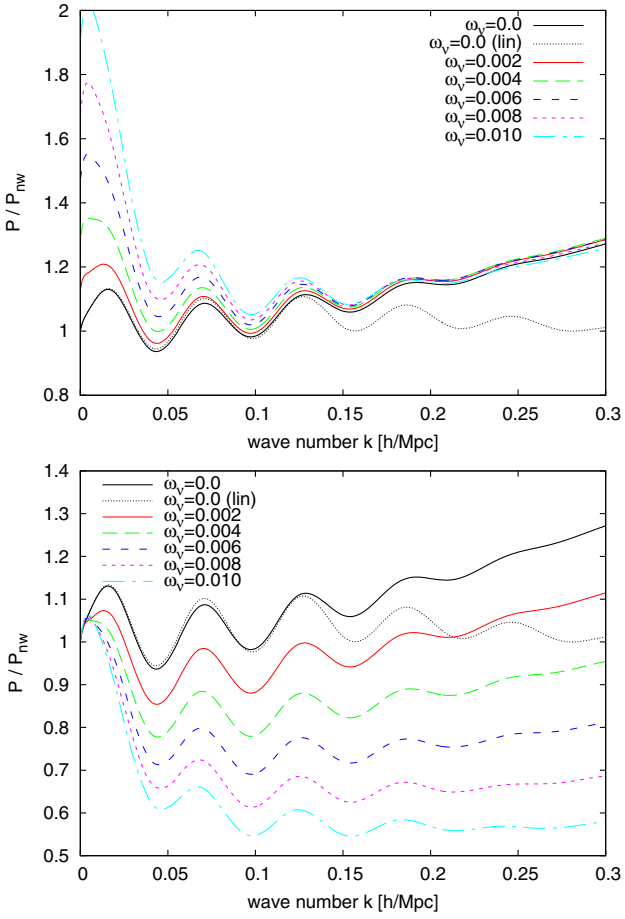

FIG. 8 (color online). Effects of varying ω_ν on the Time-RG matter power spectrum at $z = 1$. In each case the M000n0 values of ω_m, n_s, h, w_0, and w_a are assumed. Top: $\sigma_8 = 0.8$ is fixed for all of the models. Bottom: All models are normalized to the same low-k value.

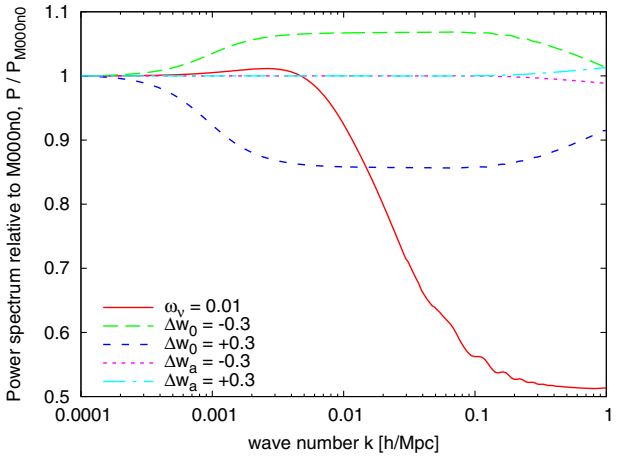

FIG. 9 (color online). Effects of varying w_0, w_a, and ω_ν on the Time-RG matter power spectrum at $z = 1$, relative to their M000n0 values. All models are normalized to the same low-k value.

Massive neutrinos shift the positions of the baryon peaks in the power spectrum, with possible implications for BAO measurements. For example, the k positions of the trough at $k \approx 0.04h$ Mpc^{-1} and the peak at $k \approx 0.07h$ Mpc^{-1} are shifted relative to the massless neutrino model in Fig. 10. Comparing the $\omega_\nu = 0$ (red, solid) and $\omega_\nu = 0.01$ Time-RG (green, long-dashed) curves in that figure, we see that neutrino masses shift the k values of these extrema by $\sim f_\nu$. Figure 10 also shows the spatial correlation function $\xi(r)$ of the matter, computed using the FFTLOG package [77]. Transformation from $P(k)$ to $\xi(r)$ requires the extrapolation of P to large k, which we do using a power law of slope $d\log P/d\log k = n_s - 3$ for linear $P(k)$ and -1 for nonlinear $P(k)$. Varying this slope by $\pm 30\%$ changes the BAO peak position by only 0.1%, so the BAO feature is robust with respect to this extrapolation.

The neutrino contribution to the power spectrum can be divided into two effects. The first is the effect of the neutrino energy density on the homogeneous expansion $H(z)$ of the universe, including the resulting effect on the CDM and baryon growth factor. The second is the direct contribution of the neutrino inhomogeneities $\delta_\nu \neq 0$ to the total matter power spectrum and to the scale-dependent growth of δ_{cb}. In order to separate these effects, Fig. 10 also shows the $\omega_\nu = 0.01$ power spectrum with the neutrino inhomogeneities set to zero, $\delta_{\nu,\mathrm{lin}} = 0$ in Eq. (19). Evidently the shifts in the baryon wiggles in the CDM power spectrum are almost entirely due to the first effect, the neutrino contribution to $H(z)$; the peak and trough positions in the Time-RG and $\delta_\nu = 0$ curves differ by ∼0.1%.

In terms of BAO analysis, this is a potentially helpful result. It implies that BAO reconstruction, which uses two-loop Lagrangian perturbation theory to map the observed density field back to the underlying linear field, can be

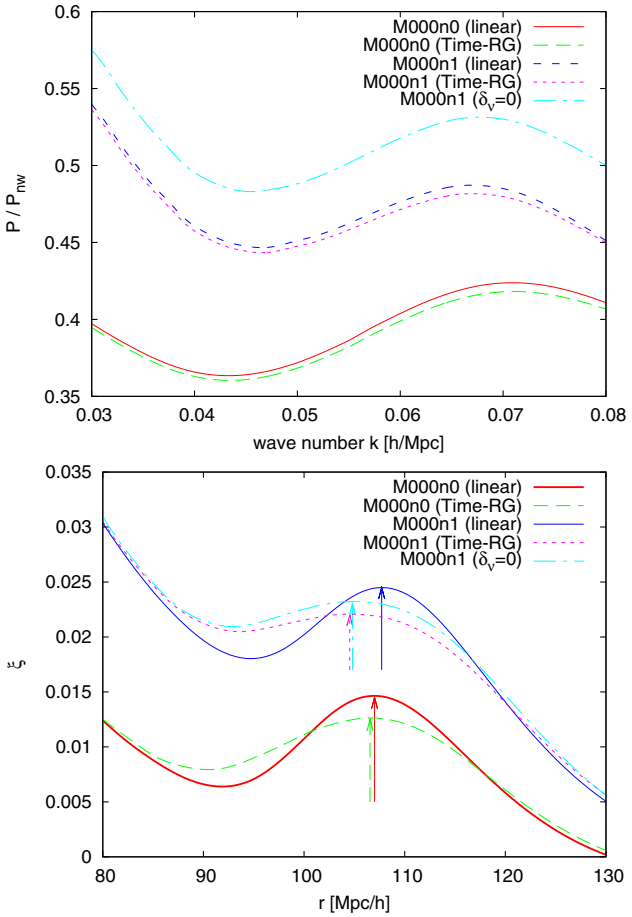

FIG. 10 (color online). Top panel: Shifts in the baryon wiggles in the matter power spectrum at $z = 1$ due to the effects of neutrino mass. Lower panel: Correlation function at $z = 1$. Vertical arrows show the locations of local extrema. The shift is almost entirely due to the neutrino contribution to the homogeneous expansion rate $H(z)$.

trivially extended to include massive neutrinos. In order to do this, one need only include the energy density and pressure of the neutrinos when computing $H(z)$ and the (scale-independent) CDM + baryon growth factor. If one approximates the BAO peak by ignoring neutrino inhomogeneities in Time-RG, then the peak position is off by less than 0.25%. This level of approximation is more than adequate for BOSS, but may become important under optimistic assumptions about DESI [27].

V. CONCLUSION

Over the next several years, surveys measuring the BAO peak and the growth of large-scale structure will provide substantially improved constraints on dynamical dark energy and massive neutrinos, especially when combined with lensing observations [27], as well as with CMB measurements. In particular, they will significantly narrow the allowed range of dark energy equations of state and will measure, rather than merely bound, the sum of neutrino masses. Analyses of these upcoming data will require a thorough understanding of the subtle effects on the matter power spectrum arising from the dark energy and neutrino sectors.

Higher-order perturbation theory and N-body simulations provide complementary predictions of the matter power spectrum, overlapping at quasilinear scales. In this work we have extended both tools to cosmologies with time-varying dark energy equations of state and massive neutrinos. By modifying the publicly available CPTER code [52], we extended several higher-order perturbation theories to cosmologies with arbitrary homogeneous evolution $H(z)$. Figure 3 and Table II compare linear theory and six different higher-order perturbation theories to N-body simulations for a ΛCDM model as well as an early dark energy. For ΛCDM (model M000n0) the higher-order calculations all agree with simulations to 2% up to $k = 0.1h$ Mpc^{-1} at $z = 0$ and up to $k = 0.15h$ Mpc^{-1} at $z = 1$; some of the perturbation theories perform substantially better than that. For early dark energy (model M001n0) the situation is similar except that two-loop SPT behaves badly at $z = 0$.

In addition to arbitrary homogeneous evolution, we included massive neutrinos, treated linearly, in the Time-RG perturbation theory. Our results in Figs. 7–8 show the effects of incrementing w_0, w_a, and ω_ν on the matter power spectrum. We find the interesting result that, on BAO scales, the neutrino contribution to the CDM and baryon power spectrum is dominated by the neutrinos' modification to the homogeneous expansion rate $H(z)$, as shown in Fig. 10. Neglecting neutrino inhomogeneities in the standard Lagrangian resummation perturbation theory reconstruction will therefore only introduce an error

TABLE III. Wave number k [h Mpc^{-1}] up to which linear and Time-RG perturbation theories are accurate up to 1% (or 2%) in models with massive neutrinos.

Model	z	Acc.	Linear	Time-RG
M000n1	0	1%	0.086	0.14
		2%	0.091	0.14
	1	1%	0.095	0.2
		2%	0.1	0.26
M000n2	0	1%	0.099	0.16
		2%	0.11	0.2
	1	1%	0.11	0.44
		2%	0.14	0.58
M001n1	0	1%	0.065	0.17
		2%	0.09	0.17
	1	1%	0.16	0.25
		2%	0.16	0.26
M002n1	0	1%	0.11	0.17
		2%	0.11	0.17
	1	1%	0.11	0.64
		2%	0.12	0.78

of $\leq 0.25\%$ in the position of the BAO peak, assuming a neutrino-to-matter ratio $f_\nu \leq 0.075$.

We added neutrinos to the HACC N-body code in a minimal fashion by neglecting the neutrino density contrast as a source for matter clustering. The matter power spectrum is found by combining the nonlinear CDM plus baryon power spectrum result along with that from neutrinos treated in linear theory. This approximation can be tested directly within Time-RG perturbation theory by neglecting the neutrino density contrast in Eq. (19). For $f_\nu = 0.075$, at $z = 0$, we find that the approximation is valid to better than 1% up to $k = 0.16h$ Mpc^{-1}, essentially the entire range of validity of perturbation theory. Since $f_\nu = 0.075$ is a few times larger than allowed by current constraints, we are justified in applying this approximation for N-body calculations. Figures 5 and 6 compare the resulting N-body power spectra to Time-RG with massive neutrinos in ΛCDM and early dark energy models, respectively. Table III summarizes the results; at $z = 0$, Time-RG and simulations agree to 2% up to at least $k = 0.14h$ Mpc^{-1} for all models considered. The combination of our Time-RG and N-body calculations is a powerful result, predicting the power spectrum in massive neutrino models, for a wide range of dark energy models, over several orders of magnitude in k.

ACKNOWLEDGMENTS

We are grateful to J. Kwan, Z. Lukić, and M. Pietroni for insightful conversations. S. H. thanks Masahiro Takada for useful discussions. The authors were supported by the U.S. Department of Energy, Basic Energy Sciences, Office of Science, under Contract No. DE-AC02-06CH11357. This research used resources of the ALCF, which is supported by DOE/SC under Contract No. DE-AC02-06CH11357 and resources of the OLCF, which is supported by DOE/SC under Contract No. DE-AC05-00OR22725.

The submitted manuscript has been created by UChicago Argonne, LLC, Operator of Argonne National Laboratory ("Argonne"). Argonne, a U.S. Department of Energy Office of Science laboratory, is operated under Contract No. DE-AC02-06CH11357.

[1] A. G. Riess *et al.*, Astron. J. **116**, 1009 (1998).
[2] S. Perlmutter *et al.*, Astrophys. J. **517**, 565 (1999).
[3] A. Vikhlinin *et al.*, Astrophys. J. **692**, 1060 (2009).
[4] A. Conley *et al.*, Astrophys. J. Suppl. Ser. **192**, 1 (2011).
[5] N. Suzuki *et al.*, Astrophys. J. **746**, 85 (2012).
[6] G. Hinshaw *et al.* (WMAP Collaboration), Astrophys. J. Suppl. Ser. **208**, 19 (2013).
[7] M. Kilbinger *et al.*, Mon. Not. R. Astron. Soc. **430**, 2200 (2013).
[8] Z. Hou *et al.*, Astrophys. J. **782**, 74 (2014).
[9] E. Calabrese *et al.*, Phys. Rev. D **87**, 103012 (2013).
[10] P. A. R. Ade *et al.* (Planck Collaboration), arXiv:1303.5076.
[11] L. Anderson *et al.*, Mon. Not. R. Astron. Soc. **427**, 3435 (2013).
[12] S. Weinberg, Rev. Mod. Phys. **61**, 1 (1989).
[13] J. Polchinski, arXiv:hep-th/0603249.
[14] S. Nobbenhuis, Found. Phys. **36**, 613 (2006).
[15] R. R. Caldwell and M. Kamionkowski, Annu. Rev. Nucl. Part. Sci. **59**, 397 (2009).
[16] J. Martin, C.R. Phys. **13**, 566 (2012).
[17] P. Binetruy, Phys. Rev. D **60**, 063502 (1999).
[18] I. Zlatev, L. M. Wang, and P. J. Steinhardt, Phys. Rev. Lett. **82**, 896 (1999).
[19] P. J. Steinhardt, L. Wang, and I. Zlatev, Phys. Rev. D **59**, 123504 (1999).
[20] C. Armendariz-Picon, V. F. Mukhanov, and P. J. Steinhardt, Phys. Rev. Lett. **85**, 4438 (2000).
[21] T. Barreiro, E. J. Copeland, and N. J. Nunes, Phys. Rev. D **61**, 127301 (2000).
[22] J. C. Bueno Sanchez and K. Dimopoulos, Phys. Lett. B **642**, 294 (2006).
[23] U. Alam, Astrophys. J. **714**, 1460 (2010).
[24] U. Alam, Z. Lukić, and S. Bhattacharya, Astrophys. J. **727**, 87 (2011).
[25] M. Ishak, A. Upadhye, and D. N. Spergel, Phys. Rev. D **74**, 043513 (2006).
[26] S. Hannestad, Phys. Rev. Lett. **95**, 221301 (2005).
[27] A. Font-Ribera, P. McDonald, N. Mostek, B. A. Reid, H.-J. Seo, and A. Slosar, arXiv:1308.4164.
[28] D. Schlegel *et al.* (with input from the SDSS-III Collaboration), arXiv:0902.4680.
[29] M. Levi *et al.* (DESI Collaboration), arXiv:1308.0847.
[30] T. Abbott *et al.* (Dark Energy Survey Collaboration), arXiv:astro-ph/0510346.
[31] P. A. Abell *et al.* (LSST Science and LSST Project Collaborations), arXiv:0912.0201.
[32] A. Refregier, A. Amara, T. D. Kitching, A. Rassat, R. Scaramella, J. Weller and f. t. E. I. Consortium, arXiv:1001.0061.
[33] T. Basse, O. Eggers Bjaelde, J. Hamann, S. Hannestad, and Y. Y. Y. Wong, arXiv:1304.2321.
[34] Y. Y. Y. Wong, J. Cosmol. Astropart. Phys. 10 (2008) 035.
[35] http://chime.phas.ubc.ca/.
[36] E. Lawrence, K. Heitmann, M. White, D. Higdon, C. Wagner, S. Habib, and B. Williams, Astrophys. J., **713**, 1322 (2010).
[37] K. Heitmann, E. Lawrence, J. Kwan, S. Habib, and D. Higdon, Astrophys. J. **780**, 111 (2014).
[38] LSST Dark Energy Science Collaboration, arXiv:1211.0310.
[39] S. Habib, A. Pope, Z. Lukić, D. Daniel, P. Fasel, N. Desai, K. Heitmann, C.-H. Hsu, L. Ankeny, G. Mark,

S. Bhattacharya, and J. Ahrens, J. Phys. Conf. Ser. **180**, 012019 (2009).
[40] A. Pope, S. Habib, Z. Lukić, D. Daniel, P. Fasel, N. Desai, and K. Heitmann, Comput. Sci. Eng. **12**, 17 (2010).
[41] S. Habib, V. Morozov, H. Finkel, A. Pope, K. Heitmann, K. Kumaran, T. Peterka, J. Insley, D. Daniel, P. Fasel, N. Frontiere, and Z. Lukić, arXiv:1211.4864.
[42] P. J. E. Peebles and B. Ratra, Astrophys. J. Lett. **325**, L17 (1988).
[43] B. Ratra and P. J. E. Peebles, Phys. Rev. D **37**, 3406 (1988).
[44] R. R. Caldwell and E. V. Linder, Phys. Rev. Lett. **95**, 141301 (2005).
[45] C. Armendariz-Picon, V. F. Mukhanov, and P. J. Steinhardt, Phys. Rev. D **63**, 103510 (2001).
[46] M. Chevalier and D. Polarski, Int. J. Mod. Phys. D **10**, 213 (2001).
[47] E. V. Linder, Phys. Rev. Lett. **90**, 091301 (2003).
[48] A. Upadhye, M. Ishak, and P. J. Steinhardt, Phys. Rev. D **72**, 063501 (2005).
[49] M. Pietroni, J. Cosmol. Astropart. Phys. 10 (2008) 036.
[50] J. Lesgourgues, S. Matarrese, M. Pietroni, and A. Riotto, J. Cosmol. Astropart. Phys. 06 (2009) 017.
[51] J. Carlson, M. White, and N. Padmanabhan, Phys. Rev. D **80**, 043531 (2009).
[52] http://mwhite.berkeley.edu/Copter.
[53] S. Pueblas and R. Scoccimarro, Phys. Rev. D **80**, 043504 (2009).
[54] P. Valageas, Astron. Astrophys. **526**, A67 (2011).
[55] S. Anselmi and M. Pietroni, J. Cosmol. Astropart. Phys. 12 (2012) 013.
[56] M. Pietroni, G. Mangano, N. Saviano, and M. Viel, J. Cosmol. Astropart. Phys. 01 (2012) 019.
[57] S. Saito, M. Takada, and A. Taruya, Phys. Rev. Lett. **100**, 191301 (2008).
[58] S. Agarwal and H. A. Feldman, Mon. Not. R. Astron. Soc. **410**, 1647 (2011).
[59] K. Abazajian, E. R. Switzer, S. Dodelson, K. Heitmann, and S. Habib, Phys. Rev. D **71**, 043507 (2005).
[60] J. Brandbyge, S. Hannestad, T. Haugbølle, and B. Thomsen, J. Cosmol. Astropart. Phys. 08 (2008) 020.
[61] M. Viel, M. G. Haehnelt, and V. Springel, J. Cosmol. Astropart. Phys. 06 (2010) 015.
[62] S. Bird, M. Viel, and M. G. Haehnelt, Mon. Not. R. Astron. Soc. **420**, 2551 (2012).
[63] A. Gardini, S. A. Bonometto, and G. Murante, Astrophys. J. **524**, 510 (1999).
[64] J. Brandbyge and S. Hannestad, J. Cosmol. Astropart. Phys. 05 (2009) 002.
[65] J. Brandbyge and S. Hannestad, J. Cosmol. Astropart. Phys. 01 (2010) 021.
[66] Y. Ali-Haïmoud and S. Bird, Mon. Not. R. Astron. Soc. **428**, 3375 (2013).
[67] N. Makino, M. Sasaki, and Y. Suto, Phys. Rev. D **46**, 585 (1992).
[68] E. V. Linder, Phys. Rev. D **72**, 043529 (2005).
[69] M. J. Mortonson, W. Hu, and D. Huterer, Phys. Rev. D **81**, 063007 (2010).
[70] A. Lewis, A. Challinor and A. Lasenby, Astrophys. J. **538**, 473 (2000).
[71] U. Seljak and M. Zaldarriaga, Astrophys. J. **469**, 437 (1996).
[72] M. Zaldarriaga, U. Seljak, and E. Bertschinger, Astrophys. J. **494**, 491 (1998).
[73] M. Zaldarriaga and U. Seljak, Astrophys. J. Suppl. Ser. **129**, 431 (2000).
[74] Y. B. Zeldovich, Astron. Astrophys. **5**, 84 (1970).
[75] K. Heitmann, M. White, C. Wagner, S. Habib, and D. Higdon, Astrophys. J. **715**, 104 (2010).
[76] A. Taruya, F. Bernardeau, T. Nishimichi, and S. Codis, Phys. Rev. D **86**, 103528 (2012).
[77] A. J. S. Hamilton, Mon. Not. R. Astron. Soc. **312**, 257 (2000).